Stability Analysis and Numerical Simulation of Multidevice Amplifiers

Motoharu Ohtomo, *Member, IEEE*

Abstract—**Stability analysis of multidevice amplifiers is made on a generalized circuit comprising two n-ports with S-matrices S (active devices) and S' (passive networks) connected at n interface ports. Open-loop transfer functions defined for a signal-flow graph and its $(n-1)$ subgraphs of incident and reflected waves at the interface ports are expressed in terms of $\det M_n$ and its minors, where $M_n = S'S - I_n$ and $I_n = n \times n$ identity matrix. It is shown that the Nyquist plots of the n transfer functions completely characterize the number of right-half complex-frequency-plane zeros of $\det M_n$, and hence the amplifier stability. Insertion of an ideal circulator and isolators at the interface ports enables one to calculate the Nyquist plots and voltage distributions of possible instabilities using commercially available linear circuit simulators. Numerical simulations for two types of parallel-operated GaAs FET amplifiers are performed to verify the usefulness of the analysis to design-phase check on multidevice amplifier stability.**

I. Introduction

ODD-mode oscillations, also called push-pull-mode or differential-mode oscillations, often cause troublesome problems to parallel-operated devices and amplifiers such as discrete power MOSFET's, internally-matched power GaAs FET's and power MMIC amplifiers [1]–[3], since this type of parasitic oscillations or instabilities not only gives rise to spurious signals but also sometimes lead to catastrophic failures of active devices [1]. In order to avoid such instabilities, design-phase analysis is very important.

Kassakian *et al.* [1] analyzed paralleled VHF power MOSFET's by postulating a differential-mode operation of the linear circuit and applying the Routh–Hurwitz criterion to its characteristic polynominal zeros. Practical use of this method, however, is limited to a case of lumped-constant circuits with relatively small number of elements. Meanwhile, Freitag *et al.* [2] analyzed cluster-matched power MMIC's with two parallel-operated GaAs FET's by assuming an odd-mode oscillation and calculating S_{11} (S -parameter) of the half circuit. This method is attractive at microwave frequencies, where lumped- and distributed-constant circuits intermingle and S-parameters are most convenient to circuit designs. Based on a signal-flow graph of S-parameters and the odd-mode assumption, Takagi *et al.* [3] analyzed the oscillations in GaAs power FET's and power MMIC amplifiers consisting of two parallel-operated FET's from the viewpoint of loop oscillation. The analysis methods in [2] and [3], however, are applicable only to a circuit configuration with symmetry, and the mode of instabilities such as the odd-mode must be postulated *a priori.* To be free from such limitations, a general yet practical approach is desirable.

This paper presents a general and comprehensive method of analyzing and simulating stability of multidevice amplifiers including parallel-operated amplifiers. In Section II, stability analysis is performed on a generalized equivalent circuit, in which two n-ports representing active devices and passive imbedding networks with S-matrices S and S', respectively, are connected at n interface ports. The circuit is viewed as a multiloop feedback system with a signal-flow graph for node signals of incident and reflected waves at the interface ports. Defining n open-loop transfer functions for the original graph and its subgraphs and obtaining explicit expressions for these transfer functions in terms of S and S', the stability of the system is analyzed from the viewpoint of the Nyquist criterion.

It is to be mentioned that the stability of a multiloop feedback system was discussed in a general manner by Mason and Zimmermann [4] using the concept of graph determinant and partial return differences for a signal-flow graph. Though very suggestive, their analysis is not applicable to a circuit analysis as in the present work where one cannot draw a full and concrete signal-flow graph of the circuit.

In Section III, numerical stability simulations of amplifiers with two and three parallel-operated GaAs FET's are given to demonstrate the usefulness of the present analysis. It is also shown that insertion of an ideal circulator and isolators at the interface ports enables us to use commercially-available linear circuit simulation softwares, thereby greatly facilitating numerical simulations.

II. Stability Analysis of Generalized Amplifier Circuit

A. Open- and Closed-Loop Transfer Functions and Nyquist Criterion

An amplifier consisting of multiple active devices and passive imbedding networks can generally be represented by an equivalent circuit as shown in Fig. 1, where n-ports with S-matrices S and S', hereafter called the n-port S and S', are connected at interface ports $1 \sim n$. Unless otherwise mentioned, we regard the n-ports S and S' as representing the active devices and the passive imbedding networks, respectively. We also regard S and S' as having no independent internal sources. Each active device can be a single- or multi-port. Without loss of generality we can

Manuscript received April 13, 1992; revised October 5, 1992.

The author is with Komukai Works, Toshiba Corporation 1, Komukai-Toshiba-cho, Saiwai-ku, Kawasaki 210, Japan.

IEEE Log Number 9208362.

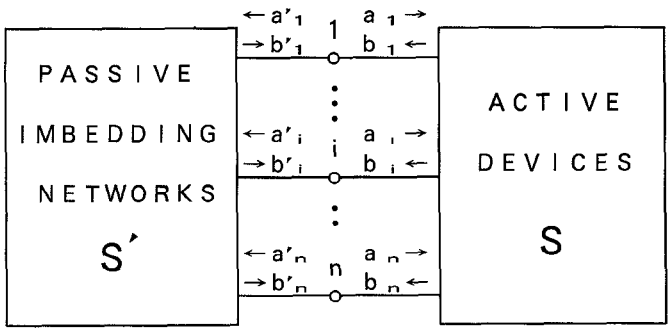

Fig. 1. Generalized equivalent circuit of multidevice amplifier, where n-ports S and S' represent active devices and passive imbedding networks, respectively.

assume that no coupling exists between active devices within the n-port S. Waves incident to and reflected from the n-ports are denoted as a_i and a_i', and b_i and b_i', respectively, at port i $(1 \leqq i \leqq n)$. Apparently, the generalized circuit defined here is the same as the generalized oscillator circuit of an n-port active device [5], [6].

Fig. 1 can be considered as a multiloop feedback system. If there is any feedback-loop instability within the system, some of the interface ports must be involved in the unstable loop, since the device activeness is the only source of instability.

If we regard $\{a_i, b_i, a_i', b_i', i = 1, 2, \cdots, n\}$ as node signals, a signal-flow graph [4] of Fig. 1 can be written as in Fig. 2, where $t_i = 1$ and $t_i' = 1$ are the transmissions or the gains of branches $b_i' \rightarrow a_i$ and $b_i \rightarrow a_i'$ $(1 \leqq i \leqq n)$, respectively. When we focus on a_i and b_i' at port i, we have a signal-flow graph of a feedback loop as shown in Fig. 3, where $G_i(s)$ is a transmission or a transfer function of the path $a_i \rightarrow b_i'$ with s as the complex angular frequency. Regarding a_i as a signal source, $G_i(s)$ is the open-loop transfer function of the feedback loop. The closed-loop transfer function $H_i(s)$ is then given by

$$H_i(s) = G_i(s)/[1 - G_i(s)]. \tag{1}$$

The open-loop transfer function defined here is equivalent to the circular function (c-function) recently introduced by Martinez *et al.* for S-parameter design of oscillators [7].

When we take a_i' as a signal source instead of a_i, we have a feedback loop similar to Fig. 3, with open- and closed-loop transfer functions $G_i'(s)$ and $H_i'(s)$. Though the paths including nodes (a_i, b_i') and (a_i', b_i) look different from the signal-flow graph point of view, consideration of only n paths containing the nodes a_i and $b_i'(i = 1, 2, \cdots, n)$ is enough to examine the amplifier stability as will be clarified later.

A necessary and sufficient condition for the feedback loop to be stable is that poles of $H_i(s)$ or zeroes of $1 - G_i(s)$ have negative real parts. The well-known Nyquist criterion is a graphical method that enables us to check the feedback loop stability from how the complex locus or the Nyquist plot of $-G_i(j\omega)$ encloses the point $-1 + 0j$ [8].

For convenience of our analysis, we will restate the Nyquist criterion in terms of $G_i(j\omega)$. Let z and p be the numbers of right-half s-plane zeros and poles of $1 - G_i(s)$, respectively. $1 - G_i(s)$ and $G_i(s)$ have the same poles. Then the number

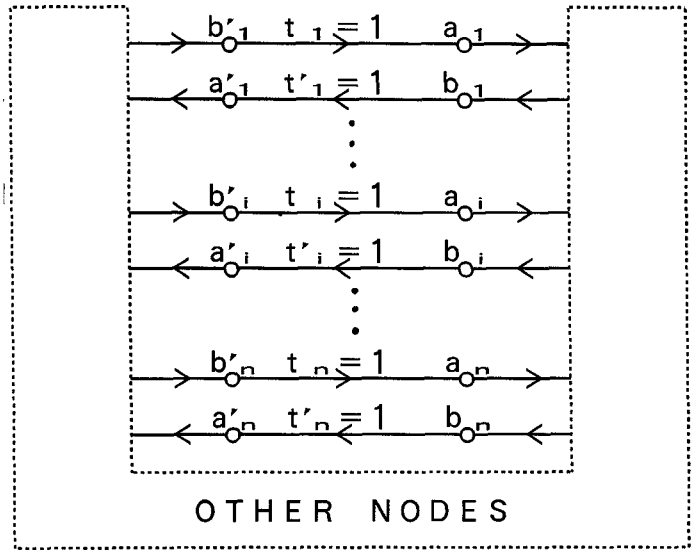

Fig. 2. Signal-flow graph of Fig. 1 with $(a_i, b_i, a_i', b_i', 1 \leqq i \leqq n)$ as node signals.

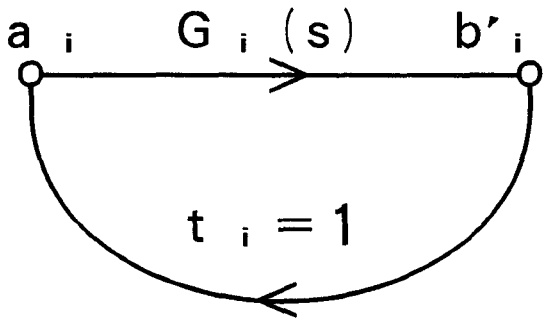

Fig. 3. Signal-flow graph of feedback loop with respect to a_i and b_i'.

N_r of clockwise revolutions around the critical point $1 + Oj$ of the Nyquist plot of $G_i(j\omega)$ for ω varying from $-\infty$ to $+\infty$ is given by

$$N_r = z - p. \tag{2}$$

Negative N_r means that the number of the counterclockwise revolutions is equal to $-N_r$. Thus, the knowledge of not only N_r but also p is required to see if z is equal to 0 or not. Since zeros and poles of a physical network function occur in complex conjugate pairs, the number of clockwise revolutions of the Nyquist plot for $\omega > 0$ $(N_r/2)$ is sufficient to apply the stability criterion and we will hereafter regard this number as N_r when we consider only positive frequencies.

When $p = 0$ is guaranteed, the system is stable if $N_r = 0$ or $G_i(j\omega)$ does not enclose the point $1 + 0j$ clockwise. Conversely the system is unstable if

$$G_i(j\omega_1), \geqq 1.$$

where ω_1 is the angular frequency at which the Nyquist plot $G_i(j\omega)$ crosses the real axis clockwise $(\arg[G_i(j\omega_1)] = 0^0$ and $-180^0 < \arg[(dG_i/d\omega)\omega = \omega_1] < 0^0)$. This corresponds to the criterion used in [2] and [3] for checking the stability of amplifiers with a single loop. In amplifiers with multiple loops, however, $p = 0$ is not always guaranteed.

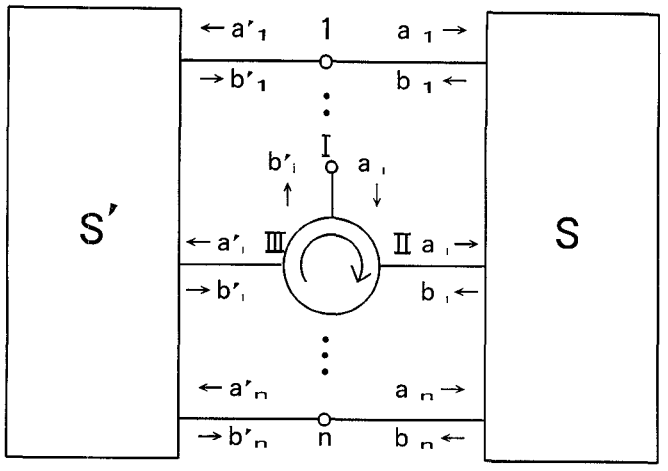

Fig. 4. Equivalent circuit corresponding to the signal-flow graph of Fig. 2 with $t_i = 0, t_k = 1$ for $1 \leqq k \neq i \leqq n$ and $t'_k = 1$ for $1 \leqq k \leqq n$.

B. Expressions of $G_i(j\omega)$ and $H_i(j\omega)$ in Terms of S and S

It can be shown that the preceding open- and closed-loop transfer functions at port i $(1 \leqq i \leqq n)$ are given as a function of $\boldsymbol{S}$ and $\boldsymbol{S}'$ by

$$G_i(j\omega) = 1 + \Delta/\Delta_{ii}(\boldsymbol{M}_n), \tag{3}$$

$$H_i(j\omega) = -[1 + \Delta_{ii}(\boldsymbol{M}_n)/\Delta], \tag{4}$$

where

$$\boldsymbol{M}_n = \boldsymbol{S}'\boldsymbol{S} - \boldsymbol{I}_n,$$

$$\Delta = \det \boldsymbol{M}_n,$$

$$\Delta_{ii}(\boldsymbol{M}_n) = \text{ cofactor of } (i,i) \text{ component of } \boldsymbol{M}_n,$$

and $\boldsymbol{I}_n$ is the $n \times n$ identity matrix. The proof of (3) is given in the Appendix. From (1) and (3) we obtain (4). The expressions for $G'_i(j\omega)$ and $H'_i(j\omega)$ can be obtained by simply interchanging $\boldsymbol{S}$ and $\boldsymbol{S}'$ in (3) and (4). Note that Δ remains unchanged since $\det(\boldsymbol{S}\boldsymbol{S}' - \boldsymbol{I}_d) = \det(\boldsymbol{S}'\boldsymbol{S} - \boldsymbol{I}_n) = \Delta$.

An equivalent circuit corresponding to the signal-flow graph in Fig. 2 with $t_i = 0, t_k = 1$ for $1 \leqq k \neq i \leqq n$ and $t'_k = 1$ for $1 \leqq k \leqq n$ is shown in Fig. 4, where the three-port circulator inserted at port i between $\boldsymbol{S}$ and $\boldsymbol{S}'$ is an ideal circulator that has S-parameters $S_{km} = 1$ for (k,m) = (II, I), (III, II), (I, III) and $S_{km} = 0$ for other (k,m). Hence, $G_i(j\omega)$ is equal to the reflection coefficient S_{II} at port I of the circulator. Such equivalence is found very convenient to the numerical simulation described in Section III, since insertion of an ideal circulator enables one to calculate $G_i(j\omega)$ using the same CAD software as for the amplifier design.

C. Open-Loop Transfer Functions in Subgraphs

If we set $t_1 = t_2 = \cdots = t_{k-1} = 0$ in Fig. 2, we obtain a subgraph [4], called here the k-th subgraph. The subgraph may retain some of the feedback loops in the original graph, With $a_1 = a_2 = \cdots = a_{k-1} = 0$, we define an open-loop transfer function denoted here as $\underline{G}_k(j\omega)$ for the path $a_k \rightarrow b'_k$ in the k-th subgraph. For $k = 1$ the subgraph is just the original graph itself, and we have $\underline{G}_1(j\omega) = G_1(j\omega)$. Then as shown

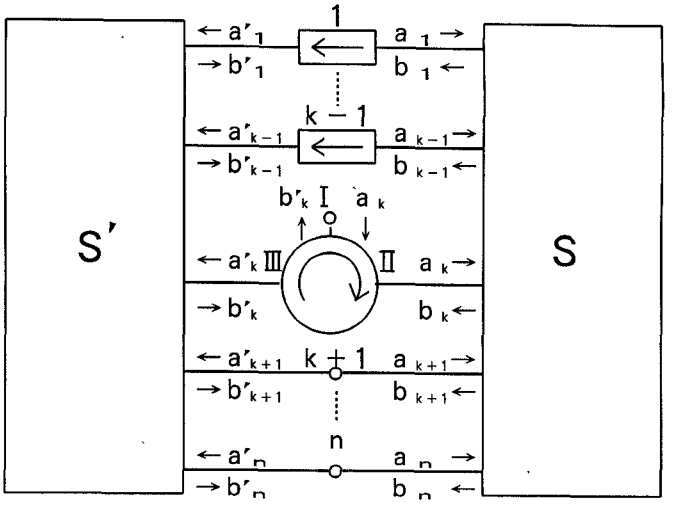

Fig. 5. Equivalent circuit corresponding to the k-th subgraph with $t_1 = t_2 = \cdots = t_k = 0$.

in the Appendix, $\underline{G}_k(j\omega)$ is given by

$$\underline{G}_k(j\omega) = 1 + \det \boldsymbol{M}_{n-k+1}/\det \boldsymbol{M}_{n-k}, \quad 1 \leqq k \leqq n, \tag{5}$$

where

$$\boldsymbol{M}_{n-k+1} = \begin{bmatrix} M_{kk} & M_{k,k+1} & \cdots & M_{kn} \\ M_{k+1,k} & M_{k+1,k+1} & \cdots & M_{k+1,n} \\ \vdots & \vdots & & \vdots \\ M_{nk} & M_{n,k+1} & \cdots & M_{nn} \end{bmatrix},$$

$$\boldsymbol{M}_0 = 1,$$

$$M_{im} = (i,m) \text{ component of } \boldsymbol{M}_n, \qquad 1 \leqq i,m \leqq n. \tag{6}$$

Since $\det \boldsymbol{M}_{n-1} = \Delta_{ii}(M_n)$, we have $\underline{G}_1(j\omega) = G_1(j\omega)$ from (3) and (5) as it should be.

An equivalent circuit corresponding to the k-th subgraph with $t_k = 0$is shown in Fig. 5, where ideal isolators (= ideal circulators with port I terminated by the reference impedance Z_0) are inserted at ports $1 \sim (k-1)$. Such insertion of ideal isolators is also utilized to calculate $\underline{G}_k(j\omega)$ in the numerical simulation.

D. Condition for Stability of Generalized Equivalent Circuit

It is usually justifiable to assume that the active devices themselves are inherently stable. Thus, all the matrix elements of $\boldsymbol{S}$ do not have poles with positive real part when viewed as functions of the complex angular frequency s. Then the matrix elements of $\boldsymbol{M}_n$ and hence $\det \boldsymbol{M}_k$ $(1 \leqq k \leqq n)$ have no pole with positive real part. Based on this assumption, the numbers, z_k and p_k, of the right-half s-plane zeros and poles of $1 - \underline{G}_k(s)$, are given from (5) as

$$z_k = z(\det \boldsymbol{M}_{n-k+1}), \tag{7}$$

$$p_k = z(\det \boldsymbol{M}_{n-k}), \tag{8}$$

where $z(\,)$ denotes the number of right-half s-plane zeros of a function in the parentheses. Hence, from (2), the number N_{rk}

of clockwise revolutions of the Nyquist plot $\underline{G}_k(j\omega)$ around $1+0j$ is given by

$$\begin{aligned} N_{rk} &= z_k - p_k \\ &= z(\det \boldsymbol{M}_{n-k+1}) - z(\det \boldsymbol{M}_{n-k}), \qquad 1 \leqq k \leqq n. \end{aligned} \tag{9}$$

By summing up N_{rk} for k from 1 to n, we obtain

$$\begin{aligned} \sum_{k=1}^{n} N_{rk} &= z(\det \boldsymbol{M}_n) - z(\det \boldsymbol{M}_0) \\ &= z(\det \boldsymbol{M}_n) = z(\Delta), \end{aligned}$$

where $z(\det \boldsymbol{M}_0) = z(1) = 0$.

Therefore, the total number N_z of the right-half s -plane zeros of $1 - G_1(s)$ is given by

$$N_z = z(\Delta) = \sum_{k=1}^{n} N_{rk}. \tag{10}$$

In the same manner, we can show that the numbers of the right-half s-plane zeros of $1-G_i(s)$ for $i \neq 1$ and $1-G_i'(s)$ for $1 \leqq i \leqq n$ are also equal to $z(\Delta)$. Hence, investigation of all the $N_{rk}'s (1 \leqq k \leqq n)$ for $G_1(j\omega)$ and $\{\underline{G}_k(j\omega), k = 2, \cdots, n\}$ suffices for determining $z(\Delta)$. Therefore, a necessary and sufficient condition for the stability of the generalized circuit in Fig. 1 is

$$N_z = \sum_{k=1}^{n} N_{rk} = 0.$$

We can also determine $z_k's$ and $p_k's$ if we know the values of all $N_{rk}'s$. From (7)–(9) we have following recursion formulas for z_k and p_k:

$$\begin{aligned} z_1 &= z(\det \boldsymbol{M}_n) \\ &= z(\Delta) = N_z, \\ p_1 &= N_z - N_{r1}, \\ z_k &= p_{k-1}, \qquad 2 \leqq k \leqq n, \\ p_k &= p_{k-1} - N_{rk}, \qquad 2 \leqq k \leqq n. \end{aligned} \tag{11}$$

As mentioned previously, the generalized circuit in Fig. 1 is the same as the generalized oscillator circuit of an n-port active device [5], [6]. In [6], the condition for an instability or oscillation to occur in such a circuit is stated as "$\det(\boldsymbol{S}\boldsymbol{S}'-\boldsymbol{I}_n)$ is nonzero and real." This, however, is incorrect, since the condition does not necessarily mean that $z(\Delta)$

So far we have assumed that the n-ports $\boldsymbol{S}$ and $\boldsymbol{S}'$ represent active devices and passive networks separately. It is evident, however, that the preceding analysis still applies even if $\boldsymbol{S}'$ contains some active devices and $\boldsymbol{S}$ some passive networks so long as the following conditions are satisfied:

i) Any instability within the system necessarily involves some of the interface ports $1 \sim n$, ii) Matrix elements of $\boldsymbol{M}_n = \boldsymbol{S}'\boldsymbol{S} - \boldsymbol{I}_n$ have no right-half s -plane poles.

Such a mixed definition of $\boldsymbol{S}$ and $\boldsymbol{S}'$ corresponds to the case reported in [3] if we let $\boldsymbol{S} = \boldsymbol{S}'$.

E. Estimation of Right-Half s-Plane Zero

As well known, if $1 - G_i(s)$ has a right-half s -plane zero, denoted here by $s_o = \sigma_o + j\omega_o (\sigma_o > 0)$, an oscillation will grow with time t in a form of $\exp[\sigma_o t + j\omega_o t]$ until linearity is no longer justified. Considering $G_i(s)$ as a regular analytic function of s, we can obtain approximate values for σ_o and ω_o from the values of $G_i(j\omega_1)$ and $(dG_i/d\omega)\omega = \omega_1$ as follows, where ω_1 is the angular frequency at which $G_i(j\omega)$ crosses the real axis. A first-order Taylor expansion of $G_i(s) - 1$ around $j\omega_1$ and substitution of $s = \sigma_o + j\omega_o$ give

$$\begin{aligned} 0 &= G_i(\sigma_o + j\omega_o) - 1 \\ &= G_i(j\omega_1) - 1 - j(dG_i/d\omega)\omega = \omega_1 \cdot [\sigma_o + j(\omega_o - \omega_1)]. \end{aligned}$$

From this we obtain, as a first-order approximation,

$$\sigma_o = -\delta \sin \theta / |dG_i/d\omega|\omega = \omega_1, \tag{12}$$

$$\omega_o = \omega_1 - \delta \cos \theta / |dG_i/d\omega|\omega = \omega_1, \tag{13}$$

where

$$\begin{aligned} \delta &= G_i(j\omega_1) - 1 \\ \theta &= \arg [(dG_i/d\omega)\omega = \omega_1]. \end{aligned}$$

F. Case of n = 2

When $\boldsymbol{S}$ and $\boldsymbol{S}'$ are two-ports ($n = 2$), we have

$$\begin{aligned} \boldsymbol{M}_2 &= \boldsymbol{S}'\boldsymbol{S} - \boldsymbol{I}_2 \\ &= \begin{bmatrix} S_{11}S_{11}' + S_{21}S_{12}' - 1 & S_{12}S_{11}' + S_{22}S_{12}' \\ S_{11}S_{21}' + S_{21}S_{22}' & S_{12}S_{21}' + S_{22}S_{22}' - 1 \end{bmatrix}, \\ \Delta &= \det \boldsymbol{M}_2 \\ &= DD' - S_{11}S_{11}' - S_{22}S_{22}' - S_{12}S_{21}' - S_{21}S_{12}' + 1, \\ \Delta_{11}(\boldsymbol{M}_2) &= S_{12}S_{21}' + S_{22}S_{22}' - 1, \end{aligned}$$

where $D = S_{11}S_{22} - S_{12}S_{21}$ and $D' = S_{11}'S_{22}' - S_{12}'S_{21}'$. Substitution of these into (3) and (5) gives the open-loop transfer functions $G_1(j\omega)$ and $\underline{G}_2(j\omega)$:

$$\begin{aligned} G_1(j\omega) &= (DD' - S_{11}S_{11}' - S_{21}S_{12}') \\ &\qquad /(S_{12}S_{21}' + S_{22}S_{22}' - 1), \\ \underline{G}_2(j\omega) &= S_{12}S_{21}' + S_{22}S_{22}'. \end{aligned}$$

Hence, from the Nyquist plots of $G_1(j\omega)$ and $\underline{G}_2(j\omega)$, we can check the amplifier stability. Conversely, these equations can be used for S-parameter design of a two-port oscillator with a feedback external to the active device.

In the case of $\boldsymbol{S} = \boldsymbol{S}'$ with each $\boldsymbol{S}$ and $\boldsymbol{S}'$ containing an identical FET, $G_1(j\omega)$ reduces to (4) of [3], in which, however, checking by $\underline{G}_2(j\omega)$ is not mentioned.

When a two-port device is terminated at its input and output ports by reflection coefficients Γ_1 and Γ_2, i.e., $S_{11}' = \Gamma_1, S_{22}' = \Gamma_2$, and $S_{12}' = S_{21}' = 0$, we have

$$\begin{aligned} G_1(j\omega) &= \Gamma_1[S_{11} + \Gamma_2 S_{12}S_{21}/(1 - \Gamma_2 S_{22})], \\ \underline{G}_2(j\omega) &= \Gamma_2 S_{22}. \end{aligned}$$

For $|\underline{G}_2(j\omega)| < 1$, the condition for instability to occur becomes

$$G_1(j\omega) = \Gamma_1[S_{11} + \Gamma_2 S_{12}S_{21}/(1 - \Gamma_2 S_{22})] > 1,$$

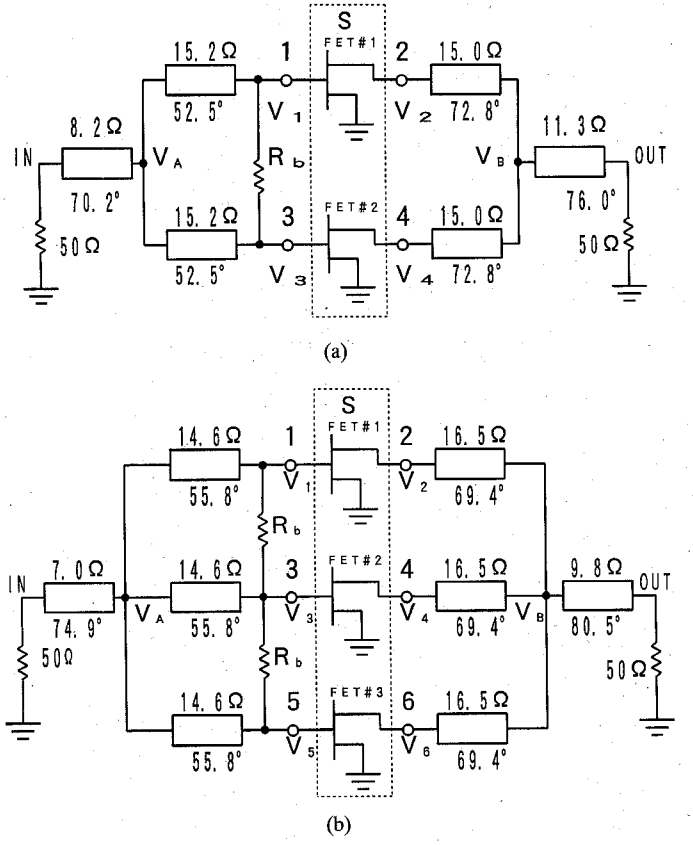

Fig. 6. Equivalent circuits of (a) type A and (b) type B amplifiers. Electrical lengths of transmission lines are defined at 10 GHz.

at a certain frequency. The threshold condition for instability is given by $G_1(j\omega) = 1$, or

$$\Delta = \Gamma_1\Gamma_2(S_{11}S_{22} - S_{12}S_{21}) - \Gamma_1 S_{11} - \Gamma_2 S_{22} + 1 = 0$$

in agreement with the oscillation threshold condition given in [9] and [5].

III. Numerical Simulation

Stability of two types of parallel-operated GaAs FET amplifiers has been numerically simulated using the HP 85150A Microwave Design System as a CAD software. Since the purpose of this section is only to demonstrate the effectivenes of the present method of stability analysis, the simulated amplifiers are of a simple configuration. Fig. 6 shows the equivalent circuits of a) type A and b) type B amplifiers tentatively designed for the simulation. The areas encircled with a dashed line represent the active devices corresponding to $\boldsymbol{S}$ in Fig. 1. Toshiba JS8853-AS medium-power GaAs FET chips for X-Ku band are used as active devices. The small-signal equivalent circuit is shown in Fig. 7. The k-factor of the device is less than 1 below 10 GHz. Though the device S -parameters calculated from the equivalent circuit are used in the present simulation, measured S-parameters can be used as well. Frequency response analysis shows that the type A and type B amplifiers have a gain $\geqq$ 8 dB for $9.14 - 10.66$ GHz and $9.12 - 10.49$ GHz with a maximum gain of 11 dB

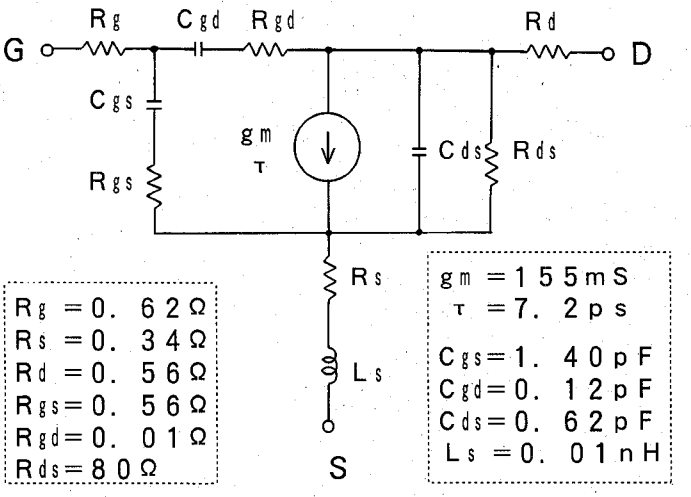

Fig. 7. Small-signal equivalent circuit of GaAs FET chip (Toshiba JS8853-AS) used in type A and type B amplifiers.

at 9.85 GHz and 9.75 GHz, respectively. The gain responses are independent of the stabilizing resistor R_b.

As mentioned in Section III, $G_1(j\omega)$ and $\underline{G}_k(j\omega)(2 \leqq k \leqq n)$ are equal to the reflection coefficient S_{11} looking from the port I of the ideal circulator inserted in the corresponding interface port as shown in Fig. 4 and 5, respectively. In the case of $\underline{G}_k(j\omega)$, ideal isolators are also inserted between $\boldsymbol{S}$ and $\boldsymbol{S}'$ at ports $1 \sim (k-1)$. Examples of the actual circuit layouts for calculating these transfer functions are shown in Fig. 8 for $G_1(j\omega)$ and $\underline{G}_3(j\omega)$ of the type A amplifier.

Type A Amplifier: Fig. 9 shows the calculated Nyquist plots of the open-loop transfer functions $G_1(j\omega), \underline{G}_2(j\omega), \underline{G}_3(j\omega)$, and $\underline{G}_4(j\omega)$ of the circuit in Fig. 6(a) with $R_b = 1 \times 10^9\,\Omega$ (virtually open). For frequencies from 0.5 to 18 GHz, only the $G_1(j\omega)$ locus encloses once the critical point $1+0j$ clockwise. Thus, we have $N_{r1} = 1$ and $N_{r2} = N_{r3} = N_{r4} = 0$, giving $N_z = z(\Delta) = 1$ from (10). Hence, the amplifier is unstable. From (11) we also have $z_1 = 1, p_1 = z_2 = p_2 = z_3 = p_3 = z_4 = p_4 = 0$.

In Fig. 9, $f_1 = 7.0714$ GHz, $G_1(j\omega_1) = 1.088$, and $(dG_1/df)_{f=f1} = 0.54e^{-j90.1^\circ}$, where $f_1 = \omega_1/2\pi$ is the frequency at which $G_1(j\omega)$ crosses the real axis. Then from (12) and (13) we obtain an approximate value of $s_o = \sigma_o + j\omega_o$, the right-half s-plane zero of $1 - G_1(j\omega)$, as $\sigma_o = 1.02 \times 10^9\,\mathrm{s}^{-1}$ and $f_o = \omega_o/2\pi = 7.0717$ GHz. Hence, an oscillation will grow with time at $f = f_o$ until linearity is no longer justified. It is worth mentioning that, if we start the stability analysis from port 2 instead of port 1, we have $f_1 = 7.0962$ GHz for $G_2(j\omega)$ which is 24.8 MHz higher than that for $G_1(j\omega)$. However, from $G_2(j\omega_1) = 1.278$ and $(dG_2/df)_{f=f1} = 2.02e^{-j78.5^\circ}$, we obtain $\sigma_o = 0.85 \times 10^9\,\mathrm{s}^{-1}$ and $f_o = 7.0687$ GHz, in a good agreement with those obtained from the $G_1(j\omega)$ locus.

Fig. 10 shows how the Nyquist plot $G_1(j\omega)$ changes with R_b. At $R_b = 240\,\Omega, G_1(j\omega) = 1$ at $f = f_1 = 7.077$ GHz. The amplifier is found stable for $R_b < 240\,\Omega$.

The rf voltages, $V_1 \sim V_4, V_A$ and V_B, at the positions indicated in Fig. 6(a) have been calculated using "the voltage probe" function furnished in the Microwave Design System.

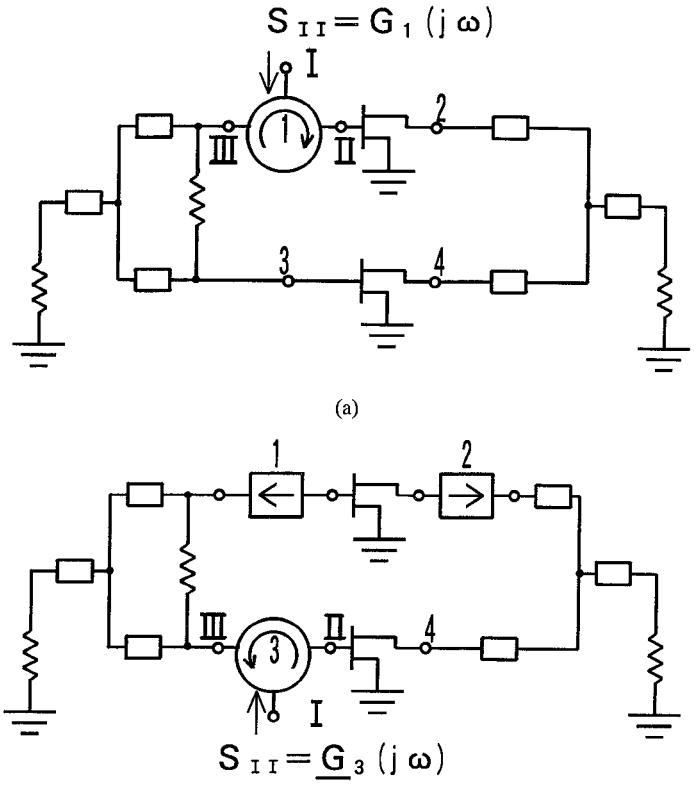

Fig. 8. Examples of circuit layout for calculating $G_1(j\omega)$ and $\underline{G}_3(j\omega)$ of type A amplifier.

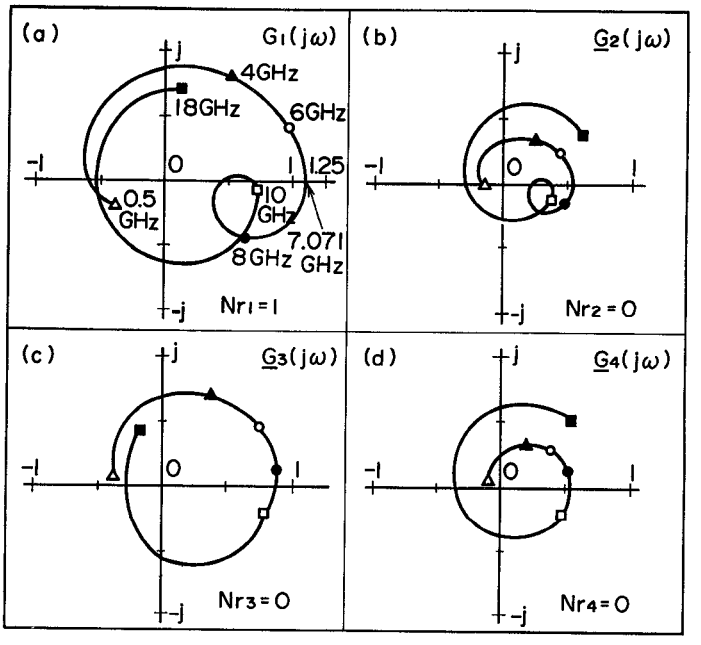

Fig. 9. Nyquist plots of open-loop transfer functions for type A amplifier calculated for 0.5 – 18 GHz. $R_b = 1 \times 10^9\ \Omega$.

The amplifier is rf-driven at $f = f_1$ through the port I of the ideal circulator inserted at port 1 to calculate $G_1(j\omega)$. Table I summarizes the calculated complex rf voltage ratios, $V_3/V_1, V_A/V_1, V_4/V_2$ and V_B/V_2. It can be seen that V_3 and

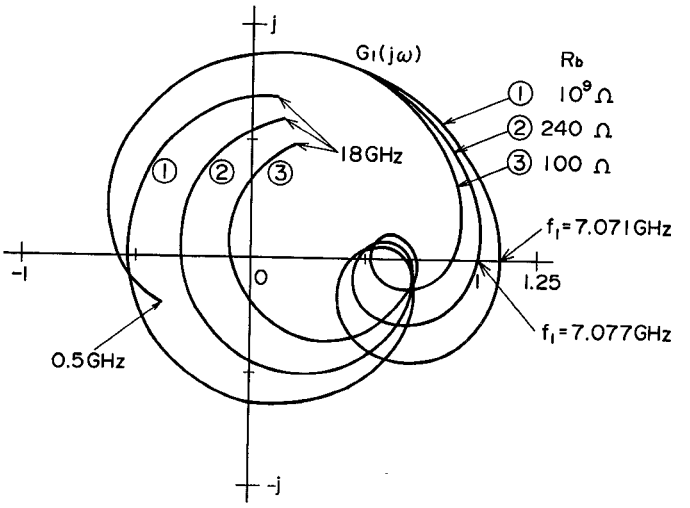

Fig. 10. Dependence of Nyquist plot $G_1(j\omega)$ on R_b for type A amplifier.

TABLE I
CALCULATED COMPLEX RF VOLTAGES IN TYPE A AMPLIFIER NORMALIZED BY V_1 AND V_2 WHEN RF SIGNAL WITH $f = f_1$ IS INJECTED FROM IDEAL CIRCULATOR INSERTED AT PORT 1 IN THE CIRCUIT OF FIG. 6(a)

R_b (Ω)	V_3/V_1	V_A/V_1	V_4/V_2	V_B/V_2
1×10^9	-1.05-0.17j	-0.01+0.06j	-1.02	-0.01+0.03j
480	-1.02-0.08j	0.03j	-1.01	0.00+0.01j
240	-1.00	0.00	-1.00	0.00

V_4 are almost completely in opposite phase with V_1 and V_2, respectively, while V_A and V_B are negligibly small in magnitude as compared to V_1 and V_2, regardless of R_b. This indicates that the instability mode of the amplifier is the odd-mode. In fact, by postulating the odd-mode oscillation in the circuit of Fig. 6(a) and analyzing half the circuit with the drain side combining point shorted as in [2], we obtained $S_{11} = 1.028\angle 180°$ at $f = 7.066$ GHz, around which oscillations could be supported. This is in excellent agreement with the simulation by our method.

Type B Amplifier: Fig. 11 shows the Nyquist plots of $G_1(j\omega), \underline{G}_2(j\omega), \underline{G}_3(j\omega), \underline{G}_4(j\omega), \underline{G}_5(j\omega), \underline{G}_6(j\omega)$ for 0.5 – 18 GHz of the type B amplifier in Fig. 6(b) with $R_b = 1 \times 10^9\ \Omega$. It can be seen that the amplifier is unstable since $N_{r1} = N_{r3} = 1, N_{r2} = N_{r4} = N_{r5} = N_{r6} = 0$, and $N_z = z(\Delta) = 2$.

The dependence of $N_{rk}(1 \leqq k \leqq 6)$ and N_z on R_b is summarized in Table II, where z_k and p_k obtained from (11) are also listed. By decreasing R_b just below 360 Ω, N_z reduces from 2 to 1. For $R_b < 120\ \Omega$ we have $N_z = 0$ and the amplifier becomes stable. It is to be noted that, with the reduction of R_b, N_{r1} changes as $1(R_b \geqq 360\ \Omega) \rightarrow 0(360\ \Omega > R_b > 300\ \Omega) \rightarrow 1(300\ \Omega > R_b \geqq 120\ \Omega) \rightarrow 0(R_b < 120\ \Omega)$, while N_{r3} changes only once from 1 to 0 at around $R_b = 300\ \Omega$. Table II also shows that only the Nyquist plots of $G_1(j\omega)$ and

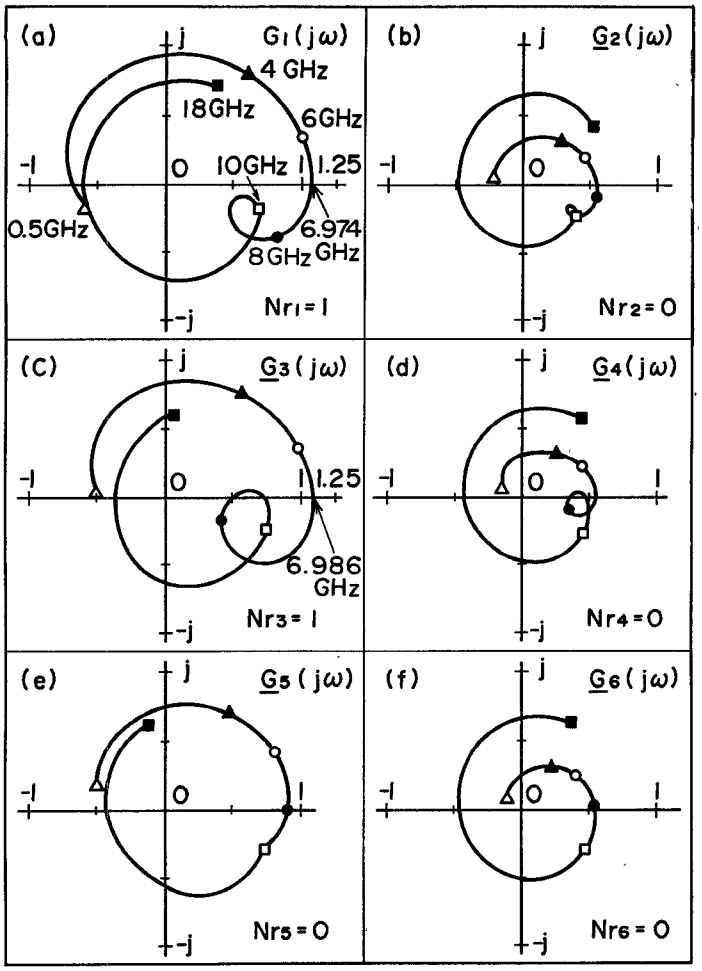

Fig. 11. Nyquist plots of open-loop transfer functions for type B amplifier calculated for 0.5 – 18 GHz. $R_b = 1 \times 10^9\ \Omega$.

$\underline{G}_3(j\omega)$ are practically enough to determine N_z in the present case.

Fig. 12 shows part of the Nyquist plots of $G_1(j\omega)$ for various values of R_b. The frequency f_1 at which $G_1(j\omega)$ crosses the real axis is 6.97 ~ 6.98 GHz for the loci ① ~ ⑤. Note the peculiarity of the loci ②, ③, and ④ near the critical point $1 + 0j$. Such behaviors can be explained by the fact that $G_1(s)$ has within itself another feedback loop whose closed-loop transfer function has an s-plane pole, $s_p = \sigma_p + j\omega_p$, near the critical point, with σ_p being positive for $R_b > 300\,\Omega$ and negative for $R_b < 300\,\Omega$.

In order to get insight into instability modes, the complex rf voltages, $V_1 \sim V_6, V_A$ and V_B at the positions indicated in Fig. 6(b) have been calculated at $f = f_1 = 6.97 \sim 6.98$ GHz in the same way as for the type A amplifier by driving an rf voltage from port 1. Table III shows the calculated rf voltages, $V_4/V_2, V_6/V_2$ and V_B/V_2 with R_b as a parameter. $V_3/V_1, V_5/V_1$ and V_A/V_1 are found almost equal to $V_4/V_2, V_6/V_2$ and V_B/V_2, respectively. From such calculations, two fundamental voltage modes for instabilities, each classified further into two types, have been identified as shown in Table IV, where the rf voltage at the output port of each FET is shown in relative magnitude and phase by the number and the ± sign, respectively. Note that FET's #1 and #3 are always electrically symmetric in Fig. 6(b).

When $R_b = 1 \times 10^9\,\Omega$ (virtually open), the instability is mode I and either type ① or type ②, since all the three FET's are electrically symmetric. Reduction of R_b begins to exclude FET #2 from such symmetry and brings about a gradual change in types and modes. By decreasing R_b to $360\,\Omega$, the instability reduces to type ② of mode I. For $R_b = 360\,\Omega$, however, the type ① of mode II prevails. At $R_b = 120\,\Omega$, below which the amplifier is stable, we have the type ② of mode II instability.

IV. Conclusion

Based on a generalized equivalent circuit, the stability of multidevice amplifiers has been discussed in a unified and comprehensive manner from the viewpoint of feedback-loop stability. By introducing open-loop transfer functions, $G_1(j\omega)$ and $\{\underline{G}_k(j\omega), k = 2, \cdots, n\}$, and expressing them in terms of the determinant and the minor determinants of $\boldsymbol{M}_n = \boldsymbol{S}'\boldsymbol{S} - \boldsymbol{I}_n$, it has been shown that the stability of the amplifiers can be completely characterized from the Nyquist plots of the n transfer functions. The analysis in this work is based on the assumptions that active devices themselves are inherently stable, no coupling exists between them within the n-port $\boldsymbol{S}$ and any feedback-loop instability can be observed at some of the interface ports. These assumptions seem to be justified in most cases.

It is also shown that insertion of an ideal circulator and isolators at the interface ports gives a practical means to calculate the Nyquist plots and the voltage distributions for possible instabilities with commercially available linear circuit simulators. The usefulness of the present analysis has been verified by numerical simulations of two types of parallel-operated GaAs FET amplifiers. The present method can be applied to stability simulations of more complexed multidevice amplifiers including distributed amplifiers and stable cascaded amplifiers. The Nyquist plots of transfer functions will enable us to visually investigate the effect of parameter changes on stability and to estimate the stability margin of the system.

Appendix

Proof of (3): The proof of (3) is given only for $i = 1$, since the proof for other i can be performed quite similarly. Keeping t'_m always equal to 1 for all $m (1 \leqq m \leqq n)$ in Fig. 2, we have

$$a'_m = b_m, \qquad 1 \leqq m \leqq n.$$

Then from the definition of S-matrices, $\boldsymbol{S}$ and $\boldsymbol{S}'$, we have

$$\begin{bmatrix} b'_1 \\ b'_2 \\ \vdots \\ b'_n \end{bmatrix} = \boldsymbol{S}' \begin{bmatrix} a'_1 \\ a'_2 \\ \vdots \\ a'_n \end{bmatrix} = \boldsymbol{S}' \begin{bmatrix} b_1 \\ b_2 \\ \vdots \\ b_n \end{bmatrix}$$

$$= \boldsymbol{S}'\boldsymbol{S} \begin{bmatrix} a_1 \\ a_2 \\ \vdots \\ a_n \end{bmatrix} = (\boldsymbol{M}_n + \boldsymbol{I}_n) \begin{bmatrix} a_1 \\ a_2 \\ \vdots \\ a_n \end{bmatrix}. \qquad \text{(A1)}$$

TABLE II
DEPENDENCE OF N_{rk}, N_z, z_k, AND p_k ON $R_b(\Omega)$ IN TYPE B AMPLIFIER ($1 \leqq k \leqq 6$)

	k	$R_b \geqq 360$			$360 > R_b > 300$			$300 > R_b \geqq 120$			$R_b < 120$		
		N_{rk}	z_k	p_k	N_{rk}	z_k	p_k	N_{rk}	z_k	p_k	N_{rk}	z_k	p_k
$G_1(j\omega)$	1	1	2	1	0	1	1	1	1	0	0	0	0
$G_2(j\omega)$	2	0	1	1	0	1	1	0	0	0	0	0	0
$G_3(j\omega)$	3	1	1	0	1	1	0	0	0	0	0	0	0
$G_4(j\omega)$	4	0	0	0	0	0	0	0	0	0	0	0	0
$G_5(j\omega)$	5	0	0	0	0	0	0	0	0	0	0	0	0
$G_6(j\omega)$	6	0	0	0	0	0	0	0	0	0	0	0	0
$N_z = \sum_{k=1}^{6} N_{rk}$		2			1			1			0		

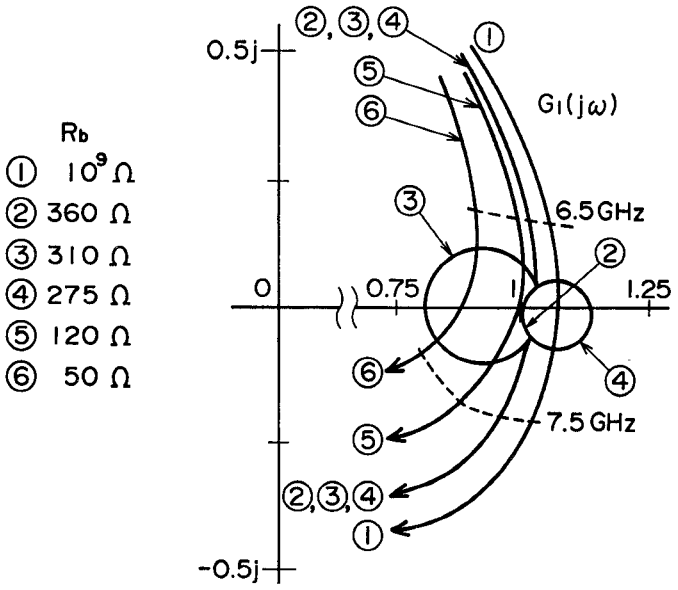

Fig. 12. Dependence of Nyquist plot $G_1(j\omega)$ on R_b for type B amplifier.

By definition $G_1(j\omega)$ is equal to b_1'/a_1 with $t_1 = 0$ and $t_2 = t_3 = \cdots t_n = 1$ in Fig. 2, and we have

$$a_m = b_m', \qquad 2 \leqq m \leqq n. \tag{A2}$$

By substituting (A2) into (A1) we obtain

$$\begin{bmatrix} b_1' \\ b_2' \\ \vdots \\ b_n' \end{bmatrix} = (\boldsymbol{M}_n + \boldsymbol{I}_n) \begin{bmatrix} a_1 \\ b_2' \\ \vdots \\ b_n' \end{bmatrix}, \tag{A3}$$

TABLE III
CALCULATED COMPLEX RF VOLTAGES IN TYPE B AMPLIFIER NORMALIZED BY V_2 WHEN RF SIGNAL WITH $f = f_1$ IS INJECTED FROM IDEAL CIRCULATOR INSERTED AT PORT 1 IN THE CIRCUIT OF FIG. 6(b)

R_b (Ω)	V_4/V_2	V_6/V_2	V_8/V_2
1×10^9	-0.51	-0.51	$0.01j$
360	$-2.03+0.01j$	$1.03+0.01j$	0.00
300	$-4.3-231j$	$3.5+232j$	$1.26+0.21j$
120	0.00	-1.00	0.00

or by rearranging

$$\begin{bmatrix} -1 & M_{12}M_{13} & \cdots & M_{1n} \\ 0 & M_{22}M_{23} & \cdots & M_{2n} \\ 0 & M_{32}M_{33} & \cdots & M_{3n} \\ \vdots & \vdots\ \vdots & \ddots & \vdots \\ 0 & M_{n2}M_{n3} & \cdots & M_{nn} \end{bmatrix} \begin{bmatrix} b_1' \\ b_2' \\ b_3' \\ \vdots \\ b_n' \end{bmatrix} = -a_1 \begin{bmatrix} M_{11}+1 \\ M_{21} \\ M_{31} \\ \vdots \\ M_{n1} \end{bmatrix} \tag{A4}$$

Solution of the linear simultaneous equations (A4) gives (3) for $i = 1$:

$$G_1(j\omega) = b_1'/a_1 = \frac{-\Delta_{11}(\boldsymbol{M}_n) - \sum_{m=1}^{n} M_{m1}\Delta_{m1}(\boldsymbol{M}_n)}{-\Delta_{11}(\boldsymbol{M}_n)} = 1 + \frac{\det \boldsymbol{M}_n}{\Delta_{11}(\boldsymbol{M}_n)}.$$

where $\Delta_{m1}(\boldsymbol{M}_n)$ is the cofactor of $(m,1)$ component of $\boldsymbol{M}_n$.

Proof of (5): By definition $\underline{G}_k(j\omega)$ is equal to b_k'/a_k with $t_1 = t_2 = \cdots = t_{k-1} = t_k = 0, t_{k+1} = \cdots = t_n = 1$, and $a_1 = a_2 = \cdots = a_{k-1} = 0$ in Fig. 2, and we have

$$a_m = b_m', \qquad k+1 \leqq m \leqq n. \tag{A5}$$

TABLE IV
VOLTAGE DISTRIBUTION MODES AND TYPES FOR INSTABILITIES IN TYPE B AMPLIFIER. THE NUMBER AND ± SIGN INDICATE THE RELATIVE MAGNITUDE AND PHASE OF THE RF V OLTAGE AT THE OUTPUT PORT OF EACH FET IN THE CIRCUIT OF FIG. 6(b)

MODE	TYPE	FET #1 (V_2)	FET #2 (V_4)	FET #3 (V_6)
I	①	± 2	∓ 1	∓ 1
		∓ 1	∓ 1	± 2
	②	∓ 1	± 2	∓ 1
II	①	0	± 1	∓ 1
		∓ 1	± 1	0
	②	± 1	0	∓ 1

Substitution of (A5) into (A1) gives

$$\begin{bmatrix} b'_1 \\ \vdots \\ b'_{k-1} \\ b'_k \\ b'_{k+1} \\ \vdots \\ b'_n \end{bmatrix} = (\boldsymbol{M}_n + \boldsymbol{I}_n) \begin{bmatrix} 0 \\ \vdots \\ 0 \\ a_k \\ b'_{k+1} \\ \vdots \\ b'_n \end{bmatrix}.$$

For $b'_k, b'_{k+1}, \cdots, b'_n$, we obtain

$$\begin{bmatrix} b'_k \\ b'_{k+1} \\ \vdots \\ b'_n \end{bmatrix} = (\boldsymbol{M}_{n-k+1} + \boldsymbol{I}_{n-k+1}) \begin{bmatrix} a_k \\ b'_{k+1} \\ \vdots \\ b'_n \end{bmatrix}, \qquad \text{(A6)}$$

where $\boldsymbol{I}_{n-k+1}$ is the $(n-k+1) \times (n-k+1)$ identity matrix. Equation (A6) can be solved for b'_k in quite the same way as solving (A3), and we obtain (5):

$$\underline{G}_k(j\omega) = b'_k/a_k = 1 + \frac{\det \boldsymbol{M}_{n-k+1}}{\det \boldsymbol{M}_{n-k}}.$$

ACKNOWLEDGMENT

The author wishes to thank N. Tomita, K. Shibata, and S. Watanabe for helpful discussions and comments.

REFERENCES

[1] J. G. Kassakian and D. Lau, "An analysis and experimental verification of parasitic oscillations in paralleled power MOSFET's," *IEEE Trans. Electron Devices*, vol. ED-31, no. 7, pp. 959–963, July 1984.
[2] R. G. Freitag, S. H. Lee, D. M. Krafcsik, D. E. Dawson, and J. E. Degenford, "Stability and improved circuit modeling considerations for high power MMIC amplifiers," in *1988 IEEE MTT-S Int. Symp. Dig.*, pp. 125–128.
[3] T. Takagi, Y. Ikeda, and S. Urasaki, "Analysis of loop oscillation for parallel running FET amplifier," IEICE, Japan, Tech. Rep., vol. 89, no. 138, MW89-59, pp. 69–74, July 1989, in Japanese.
[4] S. J. Mason and H. J. Zimmermann, *Electronic circuits, signals, and Systems*. New York: John Wiley, chs. 4, 9, 1960.
[5] A. P. S. Khanna and J. Obregon, "Microwave oscillator analysis," *IEEE Trans. Microwave Theory Tech.*, vol. MTT-29, no. 6, pp. 606–607, June 1981.
[6] R. Soares, Ed., *GaAs MESFET Circuit Design*. MA: Artech House Inc., ch. 7, 1988.
[7] R. D. Martinez and R. C. Compton, "A general approach for the S-parameter design of oscillators with 1 and 2-port active devices," *IEEE Trans. Microwave Theory Tech.*, vol. MTT-40, no. 3, pp. 569–574, Mar. 1992.
[8] J.-C. Gille, M. J. Pélegrin, and P. Decaulne, *Feedback Control Systems*. New York: McGraw-Hill, pp. 268–272, 1959.
[9] G. R. Basawapatna and R. B. Stancliff, "A unified approach to the design of wide-band microwave solid-state oscillators," *IEEE Trans. Microwave Theory Tech.*, vol. MTT-27, no. 5, pp. 379–385, May 1979.

Motoharu Ohtomo (M'91) was born in Osaka, Japan on February 11, 1938. He received the B. E. degree in applied physics from the University of Tokyo, Japan in 1960, and the Dr. Eng. degree from the same university in 1976.

In 1960 he joined Toshiba Corporation, Kawasaki, Japan. For the first several years he was mainly engaged in research and development of ruby maser. Since 1966 he has been involved in research and development of microwave semiconducator devices and circuits. He worked on Gunn-effect devices from 1966 to 1968, IMPATT and TRAPATT oscillators from 1968 to 1974, and microwave integrated circuits from 1974 to 1978 at Toshiba R&D Center. From October 1979 until now, he has been with Toshiba Komukai Works, except for two and a half years (late 1985–early 1988) at the Technical Planning & Coordination Division in the head office. In 1981 he was appointed the manager of the Microwave Solid-State Department, Komukai Works. His current interests are mainly in the field of microwave- and millimeter-wave devices and circuits.

Dr. Ohtomo is a member of the Institute of Electronics, Information and Communication Engineers of Japan.